ADVANCED MATERIALS INTERFACES
www.advmatinterfaces.de

Polarized Hydroxyapatite: New Insights and Future Perspectives Through Systematic Electrical Characterization at the Interface

Jordi Sans, Marc Arnau, Vanesa Sanz, Pau Turon,* and Carlos Alemán**

Design of hydroxyapatite (HAp) with customized electrical properties is of special interest for developing technological and biomedical applications with new improved functionalities. Polarized HAp, which is obtained by applying an external electric voltage at high temperature, has been successfully shown to be an alternative to doped-HAp that is limited by the biocompatibility of the dopants used. However, many aspects about such new material remain scarcely studied, as for example the relationship between the polarization conditions and the resultant electrical enhancement, hinder a solid progress in its application. In this work, polarized HAp has been extensively characterized using electrochemical impedance spectroscopy by means of proposing a unified electrical equivalent circuit model with physical sense. This allows to explain the properties of such material by separating the bulk and the interface contributions. Moreover, the limits of the polarization mechanism have been explored, enabling a precise control on the electrical resistivity of polarized HAp above or below the intrinsic resistivity of nonpolarized HAp. Overall, necessary insights on the polarization treatment have been reported, opening an appealing avenue for generating new biomedical and technological applications based on dopant-free polarized HAp.

1. Introduction

In the last decade, there has been a significant interest increase in connecting the electrical properties of biomaterials with their final bioactivity.[1] In fact, the study of complex biological processes in terms of surface charge accumulation or electric currents, such as cell growth, drug delivery, transfection, and production of reactive oxygen species (ROS), has been decidedly appealing in order to design new strategies to improve material properties based on fundamental knowledge.[2] Accordingly, development of biomaterials with enhanced electrical properties is much needed.

Synthetic hydroxyapatite (HAp), $Ca_5(PO_4)_3(OH)$, with enhanced electrical properties has been extensively explored.[3–5] As its open crystalline structure favors ion exchange, the incorporation of dopants into HAp is the most widely used approach to enhance the electrical properties of this ceramic. Thus, HAp-doped composites with improved osteoblast capacity,[6] anisotropic osteogenesis (by inducing a piezoelectric behavior),[7] and antibacterial response[8] have been reported. Moreover, improved conductivity and capacitances to extend the range of applications to other fields, such as bioelectromechanics,[1] corrosion,[9] and catalysis[10] have also been studied. However, this strategy presents an important drawback, which refers to the toxicity of the dopants used. For that reason, another approach, which consists on inducing electrical polarization to naked HAp by applying a polarized DC field at high temperature, has been considered.[11] Among other advantages, the increment of HAp surface charge through the thermally-stimulated polarization (TSP) process has been shown to enhance the osteobonding in bone tissues (1 kV cm^{-1} at 300 °C),[12] to improve the adsorption of inorganic phosphates (3 kV cm^{-1} at 1000 °C)[11] and to minimize the bacterial adhesion (3 kV cm^{-1} at 400 °C).[13]

When the TSP process is applied to induce permanent polarization (3 kV cm^{-1} at 1000 °C), HAp becomes catalytically active, promoting reactions that involve the CO_2 and N_2 conversion into added value chemicals.[14,15] Motivated by this important fact, we recently reported a complete polarization mechanism, which was based on direct observation of the specific orientation and amount of hydroxyl groups present in the HAp lattice.[3] Nonetheless, a comprehensive and systematic study relating the polarization conditions with the resultant electrical properties, such as conductance, capacitance, or temporal stability, has not been reported yet. Besides, results derived from characterization techniques are diverse, mostly attributed to the fact that each study considers different electrical models

J. Sans, M. Arnau, C. Alemán
Universitat Politècnica de Catalunya
Departament d'Enginyeria Química
C/ Eduard Maristany 10–14, Barcelona 08019, Spain
E-mail: jordi.sans@upc.edu; carlos.aleman@upc.edu
V. Sanz, P. Turon
B. Braun Surgical
S.A. Carretera de Terrasa 121, Rubí, Barcelona 08191, Spain
E-mail: pau.turon@upc.edu
C. Alemán
Institute for Bioengineering of Catalonia (IBEC)
The Barcelona Institute of Science and Technology
Baldiri Reixac 10–12, Barcelona 08028, Spain

The ORCID identification number(s) for the author(s) of this article can be found under https://doi.org/10.1002/admi.202101631.

DOI: 10.1002/admi.202101631

for HAp, making difficult the comparison among different investigations.[11,16] Consequently, the electrical enhancement achieved for each application remains tighten to the specific polarization conditions used.

In this work, we use the electrochemical impedance technique (EIS) as a powerful tool to explore the resultant HAp electrical properties for a wide range of polarization conditions. The main challenge to ensure proper comparison among samples resides on the determination of a reliable and reproducible electrical equivalent circuit (EEC) with physical sense. For this reason, exhaustive inspection of the HAp structural modifications, which depend on the polarization conditions, has been performed by means of Raman spectroscopy (complete mappings and in-depth sample measurements) and X-ray diffraction (XRD) analyses. Results demonstrate the achievement of major electrical enhancement through polarization at low temperature and mild voltage, even though, further refinement through increased crystallinity, temporal stability or control of the interface can be provided by increasing the temperature while the voltage is kept at moderate levels to avoid crystal lattice distortions.

2. Results and Discussion

The materials and the hydrothermal procedure used to prepare highly crystalline HAp powder are reported in the Supporting Information. After sintering for 2 h at 1000 °C, 150 mg of the obtained white HAp powder were pressed for 10 min at 620 MPa into disks of 5 mm of radius and ≈1.7 mm of thickness. Polarization of the discs was successfully achieved applying the TSP treatment. For this purpose, the discs, which were placed between two stainless steel AISI 304 electrodes, were exposed at a high voltage (from 250 to 1000 V) while applying a high temperature (from 300 to 1100 °C) for 1 h, the values of both voltage and the temperature being explicitly indicated for each case. Finally, the discs were allowed to cool down maintaining the applied electric potential for 30 min, and finally, all the system was powered off and left to cool overnight. Hereafter, HAp samples obtained after apply the TSP treatment will be denoted HAp/tsp.

2.1. Determination of the Equivalent Circuit

Based on the literature, the crystal lattice of HAp/tsp samples undergoes four major modifications with respect to nonpolarized HAp, which are responsible of its enhanced electrical properties.[3,4,15] Thus, the equivalent electrical circuit EEC has been designed considering the following four changes: (1) generation of OH^- vacancies in the lattice; (2) alignment of the OH^- dipoles, pointing towards a specific direction; (3) increase of crystallinity; and, (4) coexistence of other calcium phosphates salts at the interface. In particular, the latter deserves special attention as it might be modeled separately from the bulk (depending on the architecture of the interface) to ensure proper comparison among EIS results. This fact must not be considered as a limitation, even though several biomedical and catalytic applications have been developed from the synergies of different coexisting calcium phosphate salts.[17] Therefore, after preliminary studies (not shown), exhaustive characterization of three representative samples: sintered but nonpolarized HAp (HAp/s), HAp polarized at 500 V and 1000 °C (HAp/tsp-P1), and HAp polarized at 500 V and 1100 °C (HAp/tsp-P2), was performed focusing on their interfaces (**Figure 1**).

Figure 1a compares the XRD spectra of the three studied samples within the $2\theta = 30°–60°$ region, reflecting the crystal refinement produced by the TSP treatment. Thus, the crystallinity (χ_c; Equation S1, Supporting Information) increased from $\chi_c = 0.85 \pm 0.02$ for HAp/s to $\chi_c = 0.92 \pm 0.03$ and 0.94 ± 0.02 for HAp/tsp-P1 and HAp/tsp-P2, respectively. Although the presence of the aforementioned interface was intuited by the apparition of new peaks in the spectrum of HAp/tsp-P2, complete characterization of the interface by means of XRD was difficult due not only to the intrinsic high penetration of the X-ray but also to the fact that HAp and some calcium phosphate salts share characteristic reflections.[15] Instead, Raman spectroscopy has been reported to provide a complete and unequivocal characterization of calcium phosphate salts.[4] Figure 1b shows that HAp/s, HAp/tsp-P1 and HAp/tsp-P2 samples present the PO_4^{3-} internal modes characteristic of crystalline HAp (ν_1–ν_4). The crystallinity of the three samples was qualitatively estimated considering the full width at half maximum (FWHM) of the ν_1 peak ($FWHM_{\nu1}$), which is shown in Figure 1c. The measured $FWHM_{\nu1}$ values (6.57, 5.89, 5.85 cm^{-1} for HAp/s, HAp/tsp-P1, and HAp/tsp-P2, respectively) were in complete agreement with the XRD results. On the other hand, the peaks located at 878, 848, and 794 cm^{-1} were attributed to the HPO_4^{2-} normal vibration mode, and the POH deformation and rotation modes characteristic of brushite ($CaHPO_4 \cdot 2H_2O$), respectively.[15] Residual traces of β-tricalcium phosphate (β-TCP) and amorphous calcium phosphate (ACP) were also detected for HAp/tsp-P2, which exhibits a splitting of ν_1 at 970 and 948 cm^{-1} due to tetrahedron distortions. The apparition of such phases was associated to the phase transition from HAp to brushite at the surface.

Comparison of the ratio between the intensity of the peak at 878 cm^{-1} and the intensity of the ν_1 peak at 962 cm^{-1} ($I_{878/962}$) indicates that the presence of brushite strongly depends on the polarization conditions. Indeed, for the sample polarized using the most extreme conditions, HAp/tsp-P2, brushite vibrations dominate over HAp vibrations ($I_{878/962} > 1$), which will be properly assessed in the next section. Nonetheless, in-depth Raman studies on HAp/tsp-P2 (Figure 1d) and HAp/tsp-P1 (Figure S1, Supporting Information) demonstrate that brushite was only present at the surface regardless on the polarization conditions, as is evidenced by the clear reduction of the $I_{878/962}$ ratio and of the peaks attributed to β-TCP and ACP. Although in-depth Raman presents some disadvantages (i.e., the signal coming from the surface cannot be fully avoided, resulting in an inexact determination of the thickness of the interface), these results are fully supported by previous work in which Raman in-depth studies were successfully related to high-resolution transmission electron microscopy (HRTEM) analyses, proving that the bulk remains as both polarized and highly crystalline HAp.[4] More specifically, HRTEM images evidenced the high crystallinity of HAp/tsp-P1 (Figure S2, Supporting Information). As it can be seen, well-defined fringes at 3.4 Å, which were associated to the (002) plane of HAp, can be identified.

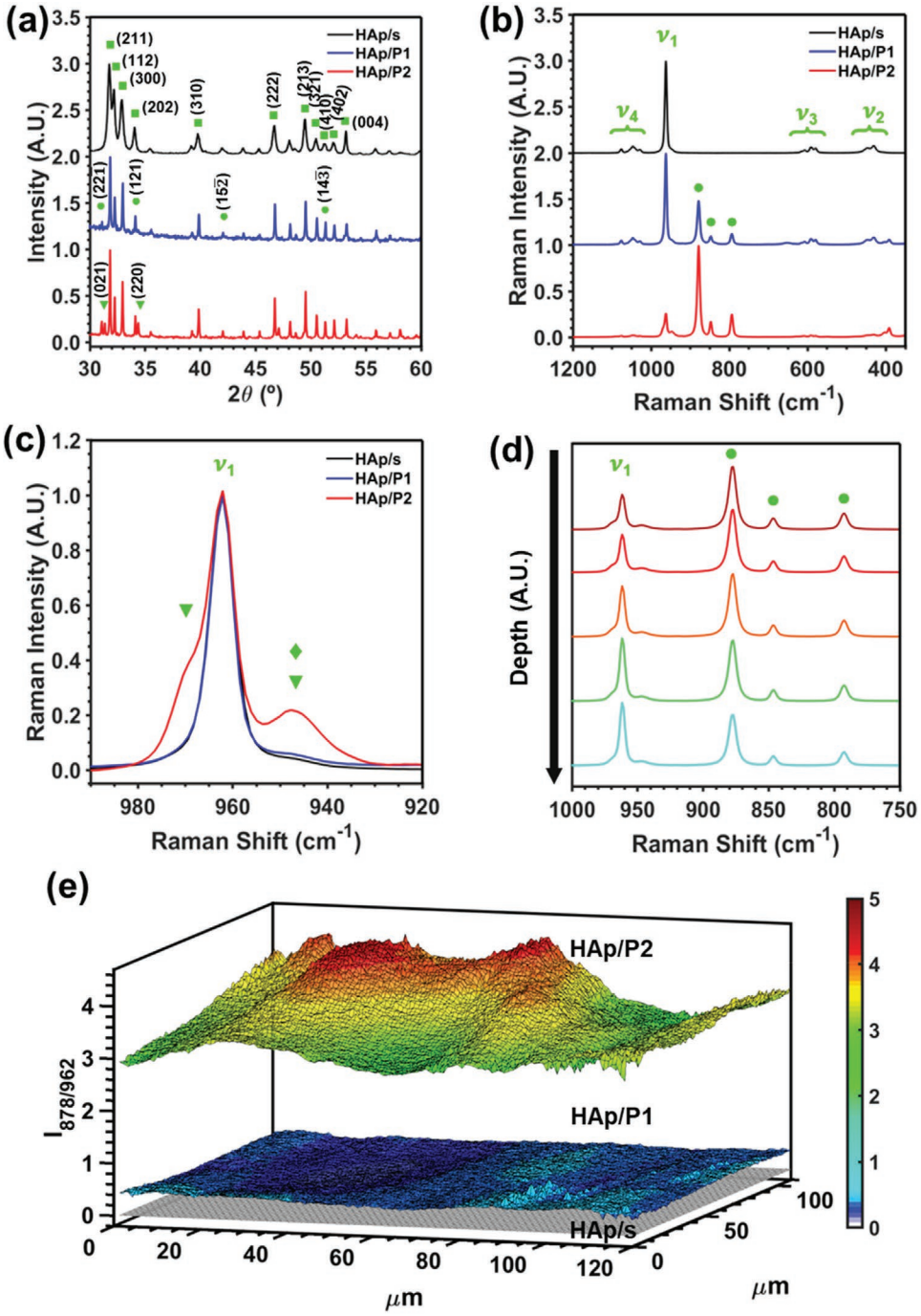

Figure 1. Structural characterization of HAp/s, HAp/tsp-P1, and HA/tsp-P2 samples. a) X-ray diffractograms in which characteristic HAp, brushite and β-TCP indexed reflections are marked with ■, ●, and ▼, respectively. Complete peak assignation is provided in the Supporting Information. b,c) Raman spectra in which (♦) accounts for ACP. d) In-depth Raman studies of HAp/tsp-P2 sample. The evolution of the HAp versus brushite composition is compared, showing that the latter decreases with increasing bulk. e) High resolution Raman mappings tracking $I_{878/962}$. Maps consist on >14 500 spectra acquired independently.

Also, additional spots appeared at 6.9 Å in the Fourier Transform image of Figure S2 (Supporting Information), which due to extinction conditions was attributed to some reorganization in the lattice structure at the interface, giving place to the formation of a larger length scale. Detailed structural discussion was provided in the HRTEM study provided in ref. [4].

On the other hand, the $FWHM_{\nu 1}$ shows almost no dependence on the different in-depth acquisitions (i.e., the standard deviation is lower than 0.008 cm^{-1}). Thus, the semi quantitative approach to crystallinity obtained by means of measuring the $FWHM_{\nu 1}$ at the surface of the sample has been considered to be representative for the whole bulk material. Finally, the Raman

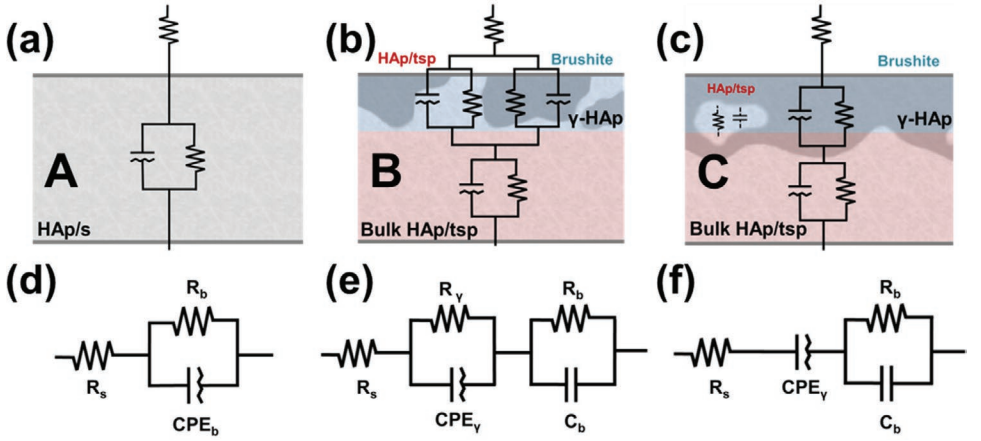

Figure 2. a–c) Scheme of the initial models considered depending on the architecture of the interface. d–f) Final simplified EECs used for fitting the experimental data.

mappings tracking $I_{878/962}$, which are depicted in Figure 1e, reveal that brushite forms an extremely heterogeneous interface across large areas, drastically increasing its presence when the temperature of the TSP treatment reaches 1100 °C.

According to the results obtained from Figure 1, the EEC was modeled evaluating separately the composition of an interface composed by HAp and brushite (hereinafter, referred as γ-HAp) and the HAp bulk. Three different cases can be distinguished: (A) initial nonpolarized HAp/s (i.e., without interface); (B) samples consisting on the polarized HAp bulk and the heterogeneous γ-HAp interface in which both the HAp and brushite contribute to the final electrical properties; and (C) polarized HAp bulk and γ-HAp interfaces in which the effect of HAp can be neglected due to the homogenization of brushite on the surface (the final average $I_{878/962}$ is higher than 1). All these considerations are graphically sketched in **Figure 2**a–c.

As an initial approach, HAp and brushite (taking into account both the bulk and the γ-HAp interface) have been modeled considering a capacitive behavior, which is usually represented by a constant phase element (CPE), in parallel with their respective resistances (CPE $\|$ R). CPEs described as $Z_{CPE} = [C\ (j\omega)^n]^{-1}$ are commonly used to replace capacitive elements (C) in real systems as they consider distortions in the capacitance due to surface roughness or distribution/accumulation of charge carriers at the grains. Thus, the parameter n of Z_{CPE} defines the capacity of retaining charges, which ranges from an ideal capacitor ($n = 1$) to a pure resistor ($n = 0$).

Further refinement of the final EEC was obtained from preliminary fits of the experimental data. Interestingly, $n \rightarrow 1$ for all circuit elements of the two the HAp/tsp samples, which is in complete agreement with the recently proposed polarization mechanism.[3] Indeed, the fact that the charge carriers are delocalized over different crystal domains reduces the capacitive imperfections due to grain boundaries, leading to an ideal capacitor behavior. For this reason, C elements have been used instead of CPE for HAp/tsp. Furthermore, the resistive component of brushite has been revised. The conductivity of HAp is provided by the OH^-, which are aligned in columns along the c-axis of the lattice (**Scheme 1**a). Conversely, brushite consists on a monoclinic structure with an *Ia* space group symmetry (Scheme 1b), in which protons are coupled to one of the oxygen of the PO_4^{3-} tetrahedra, restricting their contribution to the conductivity. Hence, the resistive branch of brushite (only when $I_{878/962} > 1$) is so large that can be neglected (open circuit). This assumption is supported by the improvement in the percentage errors associated to each circuit element (**Table 1**) with respect to the EEC that considers both the resistive and the capacitive branches (Table S1, Supporting Information).

For the sake of completeness, the same EEC was tested for HAp/tsp-P1 without showing fitting convergence (Table S2, Supporting Information), which resulted in a potential alternative method for characterizing HAp interfaces. Overall, the final simplified EECs (corresponding to cases A, B, and C, respectively) are presented in Figure 2d–f. As a general rule,

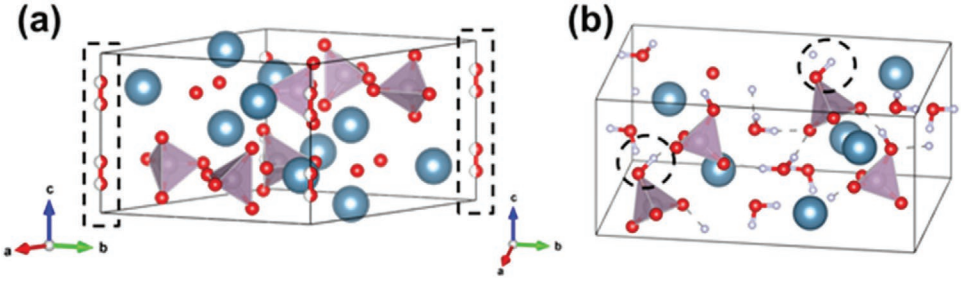

Scheme 1. a) HAp unit cell and b) Hydrated brushite unit cell. The positions of the OH^- groups are highlighted in (a) and (b) using dashed rectangles and circles, respectively.

Table 1. Data derived from experimental EIS recorded for HAp/s, HAp/tsp-P1, and HAp/tsp-P2, considering the EEC models aforementioned.

	HAp/s	HAp/tsp-P1	HAp/tsp-P2
EEC Model	Case A	Case B	Case C
R_s [Ω cm^{-2}]	40	38	44
Error [%]	2.2	2.5	2.3
R_γ [kΩ cm^{-2}]	–	9.07	–
Error [%]	–	4.84	–
CPE$_\gamma$ [μF cm^{-2} sn^{-1}]	–	100.81	110.39
Error [%]	–	1.75	3.34
n_γ	–	0.71	0.74
Error [%]	–	0.27	0.51
R_b [MΩ cm^{-2}]	9.69	1.57	1.10
Error [%]	4.81	5.00	4.70
C_b [μF cm^{-2} s^{-1}]	2.22 n = 0.83 (CPE)	12.16	16.14
Error [%]	0.49 0.09	0.66	0.76

the circuit elements have been indexed as "b" or "γ" depending on whether they correspond to the bulk or the γ-HAp interface, respectively. Thus, in the EEC displayed in Figure 2d, R_b and CPE$_b$ refer to R_{HAp} and CPE$_{HAp}$, respectively; in Figure 2e, CPE$_\gamma$ and R_γ correspond to CPE$_{brushite} \| C_{HAp}$ and $R_{brushite} \| R_{HAp}$, respectively; in Figure 2f, CPE$_\gamma$ indicates CPE$_{brushite}$; and R_s is the electrolyte resistance in all EECs (Figure 2d–f).

Experimental data and their corresponding fits using the proposed EECs are shown in **Figure 3**, which displays both the Nyquist and Bode plots. The agreement between the experimental and fitted profiles was excellent in all cases, the shape of the profiles obtained for HAp/tsp-1 and HAp-tsp2 being similar. Instead of the semi-circular response typically associated to the electrode-solid disk interface, capacitive spikes were expected in the Nyquist plot due to the fast charge transport propitiated by the wetted samples. Indeed, the slope of the polarized samples approached the imaginary axis, reflecting the aforementioned capacitive behavior.[11,18] At high frequencies, the phase of the Bode plots of HAp/tsp-P1 and HAp/tsp-P2 shows a value close to 0° rather than to 80°, as is characteristic for resistive materials in the dry state. It is worth remarking that the double-layer capacitance associated to the liquid electrolyte, which was considered in the EEC models analyzed in Figure S3 and Table S3 (Supporting Information), provided not only worse statistical errors but also results without physical meaning nor convergence, suggesting that such elements can be neglected. Actually, this was not an unexpected result since previous EIS measurements of the electrolyte alone (used as control, Figure S4, Supporting Information) showed negligible values compared with the other circuit elements. Moreover, few electrolyte droplets are applied in the samples under study as compared with the control.

Table 1 indicates that all circuit elements display error percentages lower than 5%, stressing out the reliability of the models proposed in this work. As it can be seen, the TSP treatment results in a considerably reduction of R_b while C_b increases substantially. Besides, CPE$_\gamma$ >> C_b, which has been attributed in part to the partial contribution of brushite (i.e., CPE$_\gamma$ are similar for HAp/tsp-P1 and HAp/tsp-P2) but mainly to the fact that the TSP treatment delocalizes the charge carriers of the bulk that accumulate at the surface of the samples. Indeed, R_γ provides an indirect description of the HAp/Brushite composition at the interface, increasing with the amount of brushite phase. Therefore, we have successfully standardized the EEC models for HAp/s and HAp/tsp, which are able to distinguish between the superficial effects and the electrical improvement of the bulk, allowing a proper comparison between different polarization conditions.

2.2. TSP: Effect of Voltage and Temperature

The effect of voltage and temperature on the final electrical properties and temporal stability was evaluated considering three sets of samples, which differ in the experimental conditions applied during the TSP process: (1) HAp/tsp prepared

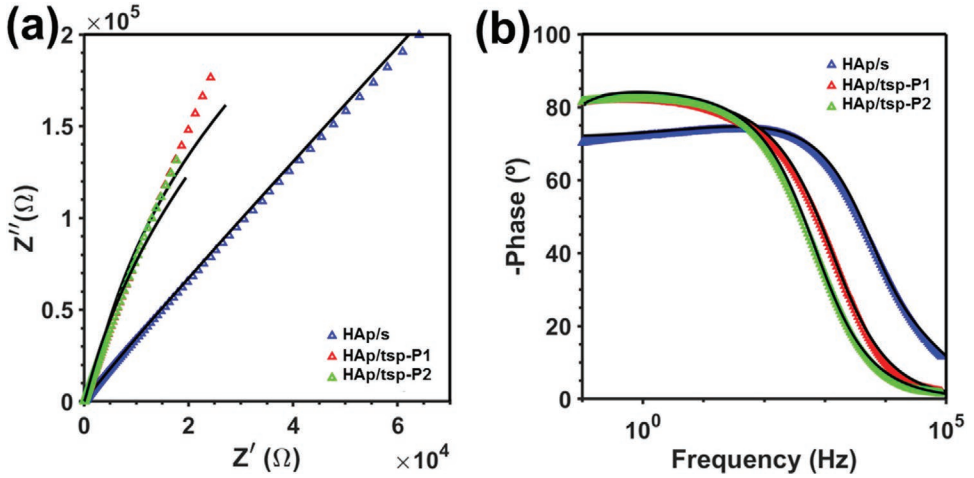

Figure 3. a) Nyquist and b) Bode plots obtained for HAp/s, HAp/tsp-P1, and HAp/tsp-P2 samples.

using a voltage of 250, 500, 750, or 1000 V at 1000 °C; (2) HAp/tsp obtained by applying a voltage of 500 V at 300, 800, 1000, or 1100 °C; and (3) HAp/tsp achieved using a voltage of 1000 V at 300, 800, 1000, or 1100 °C. EIS assays were conducted for all samples and results were fitted with the EEC models proposed in the previous section. The model was selected according to the composition of the γ-HAp: Case B for $I_{878/962} < 1$ and Case C for $I_{878/962} > 1$. The values for the circuit elements and their corresponding statistical errors are listed in Tables S4–S6 in the Supporting Information.

With respect to HAp/s, the TSP treatment produces electrical enhancement at the bulk level for mostly all the studied conditions. However, no clear trend is observed for either voltage (**Figure 4**a) or temperature (Figure 4b) variations, unless crystallinity is considered through the $FWHM_{\nu 1}$ (Figure 4c,d). This fact supposes a clear change of paradigm since the different TSP conditions do not affect to the quality of the hydroxyl reorientation, which is responsible for the improvement in the electrical properties, but to the ability of the rest of species in the lattice to reduce the imperfections caused by such reorientation. Although both R_b and C_b follow the same behavior (i.e., strong dependence on the crystallinity), charge accumulation mechanisms are more sensitive to the generation of OH^- vacancies, grain boundary effects and charge migration towards the surface (responsible of the polarization mechanism). Thus, changes in the C_b values are expected to be larger than in R_b when the different TSP conditions are applied. Despite of this, it must be emphasized that the bulk resistive behavior determines the delocalization and accumulation of charges at the HAp interface, playing a crucial role in biomedical and catalytic applications.

At temperatures lower than 1000 °C, the energetic threshold needed for crystal refinement can be exceeded by increasing the voltage. Thus, the R_b and $FWHM_{\nu 1}$ of samples polarized at 1000 V and 800 °C are similar to those of samples obtained at 500 V and 1100 °C (Figure 4b,d). Thus, the PO_4^{3-} tetrahedra and Ca^{2+} distortions caused by increasing the voltage when the mobility of species is favored by the temperature, which is achieved above 800 °C,[3] results in worsening the electrical properties (Figure 4a). Accordingly, the thermal degradation of HAp, which naturally occurs above 1100 °C,[19] seems to start at 1000 °C when a voltage of 1000 V is applied (Figure 4b). It should be noted that data obtained at 1100 °C and 1000 V must be considered with caution since the samples presented high content of β-TCP phase (Figure S5, Supporting Information), which was not considered in the EEC. On the other hand, increasing the temperature while maintaining the voltage at moderate values, as for example 500 V (Figure 4b), appears to be the most desirable to achieve the highest electrical enhancement. This is because the crystallinity and the electrical properties increase linearly with the temperatures above 800 °C.

As it can be seen in **Figure 5**a,b, major lattice rearrangements in form of brushite can be observed above 800 °C. Both

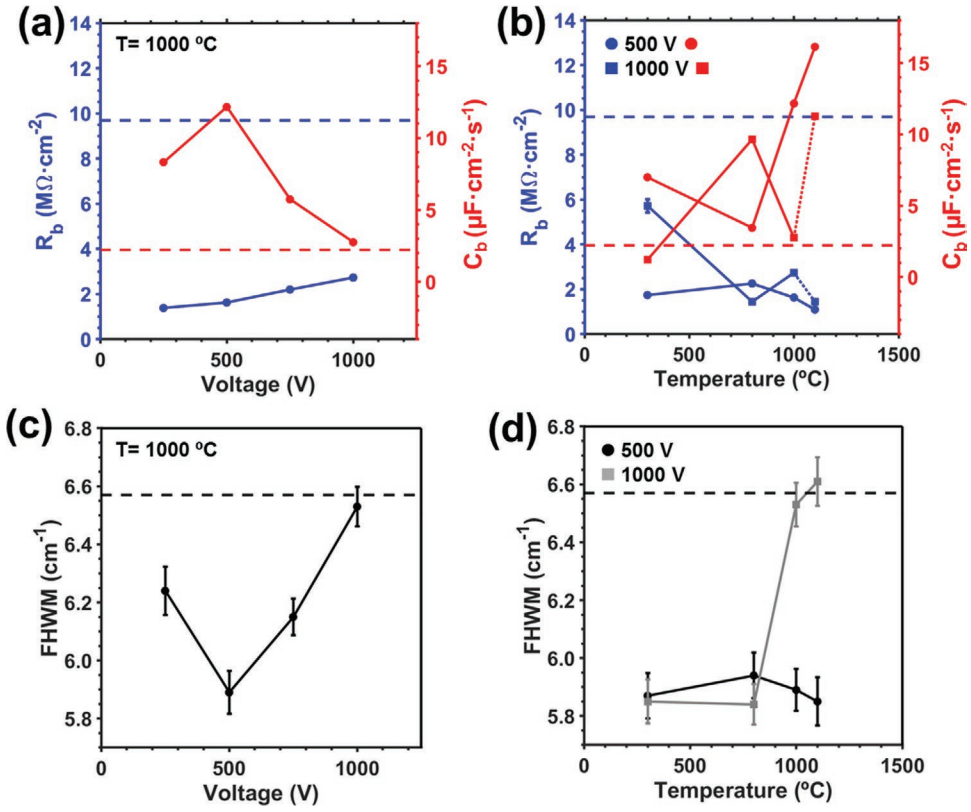

Figure 4. Effect of the a,c) voltage and the b,d) temperature on the a,b) electrical properties of the bulk and the c,d) $FWHM_{\nu 1}$ (i.e., crystallinity) for HAp/tsp samples prepared using different experimental conditions. Error bars in (a and b) are smaller than the graph points. The electrical parameters and the $FWHM_{\nu 1}$ obtained for the HAp/s are represented by dashed lines (reference).

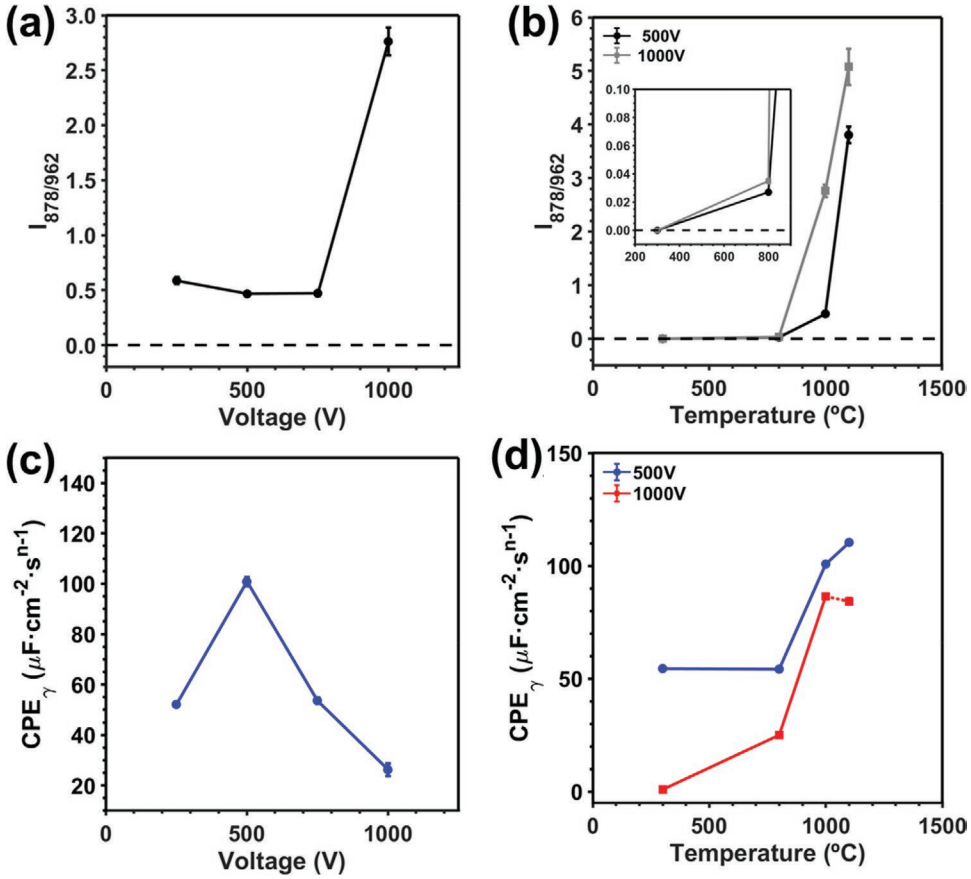

Figure 5. Effect of the a) voltage and the b) temperature on the average brushite content ($I_{878/962}$). Effect of the c) voltage and the d) temperature on the capacitance at the interface. The circuits corresponding to cases B and C (Figure 2) were considered for $I_{878/962} < 1$ and > 1, respectively. The parameters obtained for HAp/s (reference) are indicated by dashed lines in (a) and (b). Error bars are smaller than the graph points.

temperature and voltage play important roles in controlling the γ-HAp interface architecture. The former allows overcoming the energy threshold needed for the mobility of species (Figure 5b) and the latter apparently controls the brushite/HAp content (Figure 5a,b). Although the presence of brushite clearly contributes to increase CPE_γ (Figure 5d), the dependence of the capacitance at the interface on the crystallinity (Figure 5c) supports the TSP mechanism aforementioned. Accordingly, in general terms the capacitive values are much higher at the interface than at the bulk.

The electrical properties of the TSP treatment through time (i.e., the temporal stability) were examined considering the proposed EECs. Results depicted in **Figure 6** confirm that the permanent polarized state, which is defined when the polarization remains for 120 d, is only reached when the temperature of the TSP treatment is, at least of, 1000 °C. More specifically, R_b increases by 540% (almost recovering the values found for HAp/s) for samples treated at 300 °C and 500 V (Figure 6a), whereas C_b decreases by 79% and 56% for samples treated at 300 and 800 °C using 500 V, respectively (Figure 6b). The fact that the capacitance is even lower than for HAp/s might be attributed to the reduction of the OH^- vacancies in the lattice due to water absorption. The evolution of the rest of the elements is provided in Table S7 (Supporting Information) Interestingly, Figure 6c reveals that samples treated at temperatures below 1000 °C loss their ideal behavior as a capacitors, which is in turn an evidence of the OH^- relaxation (i.e., dipole pointing to unspecific directions) while the crystallinity remains unaltered. In absence of specific OH^- orientation, electric charges cannot move freely across different crystalline domains resulting in the "electrical leakages" modeled by the CPE element. It is worth mentioning that a permanent stability of the γ-HAp interface was not achieved for any of the tested conditions (Figure S6, Supporting Information). A decrease in the brushite content was observed after 60 d, even though successful full recovering of the initial interface by applying the TSP treatment was obtained.

Overall, systematic studies of the conditions used for the TSP treatment allow concluding: (1) In the short term, a major enhancement of the electrical properties is obtained by applying mild TSP conditions; (2) further enhancement of the electrical properties is achieved when increasing the crystallinity of the samples by modifying the TSP conditions; (3) Increasing the temperature is more effective compared to changing the voltage; (4) The architecture of the brushite/HAp interface, which is formed at temperatures above 800 °C, can be controlled by regulated through the applied voltage; and (5) 1000 °C are required for reaching and prolonging through time the permanent polarized state.

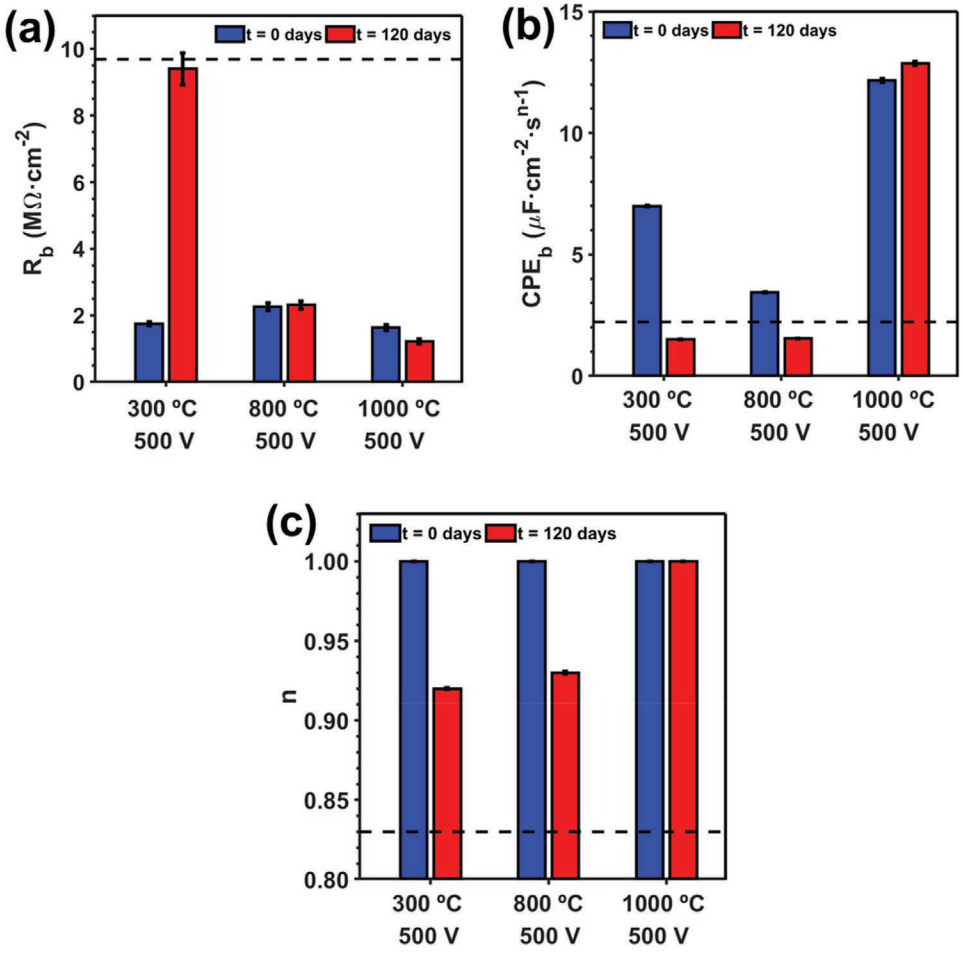

Figure 6. Temporal studies of the most representative samples. After 120 d, a) the bulk resistance, b) real capacitance, and c) *n* factor are compared. The electrical parameters obtained for HAp/s (reference) are represented by dashed lines.

2.3. Confirmation of the TSP Mechanism through Exotic Polarizations

In this section, different non-conventional TSP treatments, hereafter referred as exotic polarizations, have been applied to confirm and exploit the limits of the TSP mechanisms proposed in the literature.[3,20]

First, the effect of placing both electrodes in contact with the mineral, as compared with the standard TSP configuration in which the positive electrode is separated by 4 cm, was studied (**Figure 7**a). Due to the change on the electrodes distance, the voltage of the former was adjusted to ensure comparable conditions (i.e., 500 V and 1000 °C). The resulting R_b values, which are compared in Figure 7b (1.24 and 1.49 MΩ cm^{-2} for "separated" and "in contact" samples, respectively), confirms that the TSP mechanism is entirely based on electrostatic forces rather than other electrochemically based mechanisms. The rest of the circuit elements (case B) are listed in Table S8 in the Supporting Information. Hence, no electrical current flow through samples was needed for the electrical enhancement. In agreement with the literature, the brushite content observed in Figure 7c was almost zero for the "in contact" sample. Therefore, explicit control on the brushite content at high temperatures can be obtained independently on the final improved electrical properties. This is of special interest for biomedical or catalytic applications that require both high crystallinity and specific control of the interface composition.

On the other hand, TSP treatments with specific OH^- global orientations have been imposed by placing the sample perpendicular to the electrodes (**Figure 8**). The idea behind this exotic polarization is to prove that HAp presents electrical anisotropy, as the direction of the OH^- columns must be parallel to the direction of the measured electrical current (Figure 8a). The electrical resistance in samples with the TSP treatment applying a "orthogonal" configuration exhibited an outstanding increment of 15 times with respect to the "parallel" configuration (i.e., R_b = 19.59 and 1.24 MΩ cm^{-2}, respectively), as is shown in Figure 8b. Moreover, the sample prepared using the "orthogonal" configuration was twice that of nonpolarized HAp/s (i.e., R_b = 9.96 MΩ cm^{-2}). Indeed, the rest of elements of the fitted circuit (case B), which are listed in Table S9 (Supporting Information), also showed significant worsening (e.g., R_γ = 3.91 MΩ cm^{-2}). Even though both surfaces of the "orthogonal" sample were exposed during the TSP treatment, they showed zero brushite content ($I_{878/962}$ = 0, Figure 8c). This result evidence that the stabilization of the brushite crystal

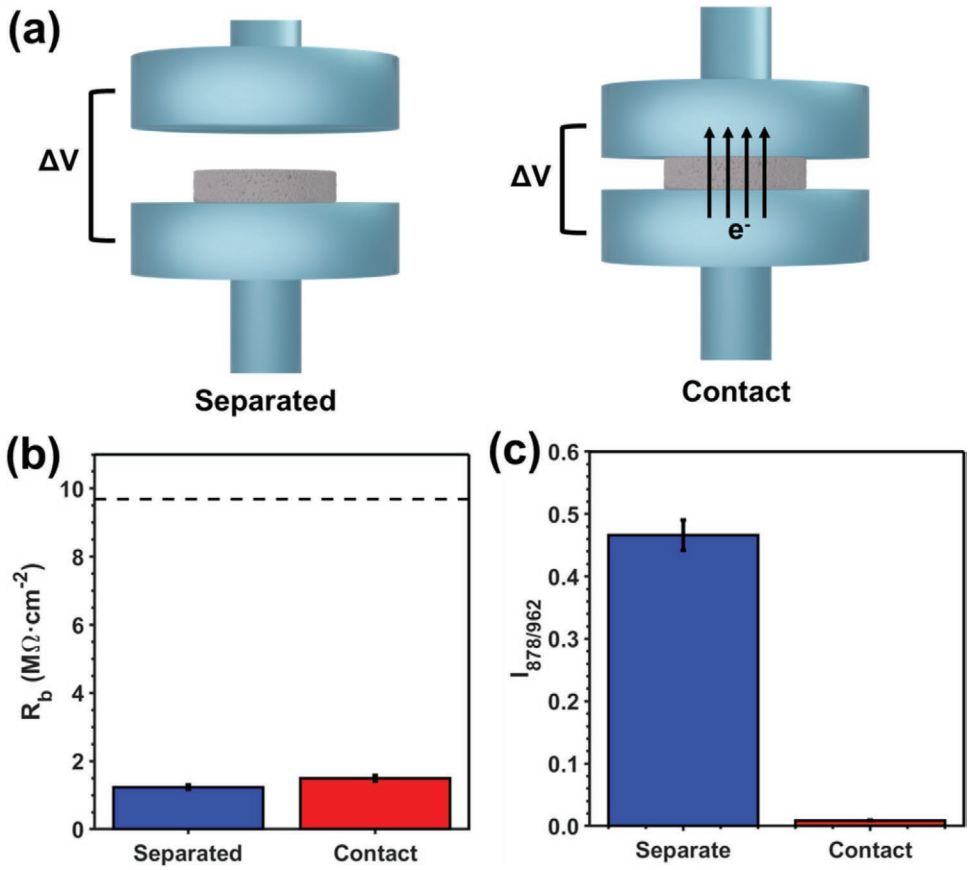

Figure 7. Exotic polarization results. a) Scheme of the TSP treatment considering "separated" and "in contact" electrodes. Comparison of b) the electrical bulk resistance and c) the $I_{878/962}$ ratio.

lattice requires a proper OH^- rearrangement (imposed by the direction of the voltage) in the H_2O positions.

Summarizing, for the first time it has been reported a treatment able to fully customize the electrical resistance of HAp without the use of dopants, including both enhancement and reduction of the conductivity, which pawns the way for the development of biocompatible nano- and micro-electromechanical systems with selective surfaces, electronic devices, catalysts, and highly selective sensors or selective cell growth applications. Some of the applications aforementioned are currently under study.

3. Conclusion

In this work we have developed a reliable electrical equivalent circuit model for HAp/tsp with physical sense based on experimental evidence. Distinction between the contributions of the bulk and the interface generated when the TSP treatment is applied (referred as γ-HAp due to the co-existence of other calcium phosphate phases) allows proper and systematic comparison among the different experimental conditions (i.e., voltage and temperature) used for the TSP treatment.

Exhaustive characterization of the electrical properties of HAp/tsp allowed us to confirm that no harsh conditions are needed to induce short term electrical enhancement, which results of special interest for standardizing TSP treatments for biological purposes using low temperatures and voltages. On the other hand, the increase of temperature is preferable to the voltage since an additional electrical enhancement is achieved by increasing the crystallinity of the samples, while once the OH^- groups have been ordered, the increase in voltage only favors the distortions of the crystal lattice. In this context, permanently polarized HAp/tsp is only achieved when the temperature of the TSP treatment reaches 1000 °C. The architecture of the γ-HAp interface, useful for both biological and catalytic applications has also been characterized in terms of TSP conditions.

Finally, the limits of the TSP treatment and the polarization mechanism have been explored, reporting for the first time a treatment that is able to completely customize the electrical properties of HAp. This ranges from high electrical resistivity, compared to nonpolarized HAp/s, to low electrical resistivity and enhanced electrical capacity behavior. Overall, this work provides the necessary tools for systematically developing and characterizing electrical customized HAp applications through the polarization mechanism. Besides, the wide range and precise control on the electrical properties pawn the way to a new generation of dopant-free polarized HAp for biocompatible applications in the fields of bioelectronics (such as the development of nano- and micro-electromechanical systems with selective surfaces or highly selective sensors) and tissue engineering, among others.

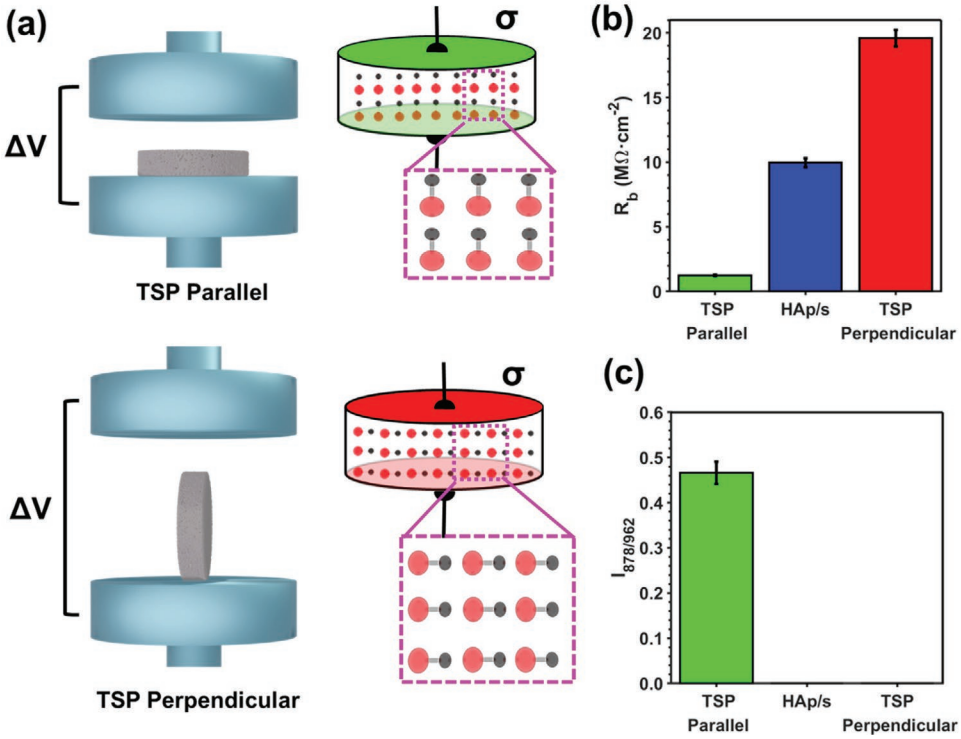

Figure 8. Exotic polarization results. a) Scheme of the studied configurations using for the TSP treatment (500 V, 1000 °C): Global parallel and orthogonal OH^- orientations have been imposed. Comparison of b) the electrical bulk resistance and c) the brushite content for the polarized samples, as determined using the procedures indicated in the Experimental Section.

4. Experimental Section

Synthesis of Electrically Enhanced HAp through the TSP Treatment: Highly crystalline HAp was obtained by hydrothermal synthesis followed by sintering treatment at 1000 °C. All details are provided in the Electronic Supplementary Information. The TSP treatment was applied by compressing the HAp powder obtained into pellets and submitting it to different electric potentials (from 250 to 1000 V) and temperatures (from 300 to 1100 °C). Details on the TSP set-up are provided in the Supporting Information. In brief, a voltage source connected to platinum wires was used in conjunction with a Carbolite muffle. Samples were placed between two stainless steel AISI 304 electrodes, which were separated 4 cm, while applying temperature.

Characterization of the Samples: EIS studies were conducted on polarized HAp pellets using a Multi Autolab/M101 from Metrohm and connected to a conductivity meter cell consisting in a two stainless steel electrodes AISI 304 plates isolated by a resin holder.[21] EECs were obtained by fitting the experimental data. In order to obtain proper EEC models, exhaustive characterization of the surface and bulk of the samples was performed by means of Raman microscopy and XRD techniques. In addition of the statistical error associated to each circuit element, the convergence of the EEC, which is based on the maximum variation of the quadratic least square error, was calculated for all the studied models. Unless specified, EEC models were validated or discarded considering such convergence criterion as a quality parameter. All the details are provided in the Supporting Information.

Supporting Information

Supporting Information is available from the Wiley Online Library or from the author.

Acknowledgements

Authors acknowledge MINECO/FEDER (RTI2018-098951-B-I00), the Agència de Gestió d'Ajuts Universitaris i de Recerca (2017SGR359), B. Braun Surgical S.A. and B. Braun Melsungen A.G. for their financial support.

Conflict of Interest

The authors declare no conflict of interest.

Data Availability Statement

The data that support the findings of this study are available from the corresponding author upon reasonable request.

Keywords

brushite, catalysis, dopant-free hydroxyapatite, electrical properties, thermally-stimulated polarization

Received: August 28, 2021
Revised: November 15, 2021
Published online: January 2, 2022

[1] A. Das, D. Pamu, *Mater. Sci. Eng., C* **2019**, *101*, 539.
[2] a) G. Singh, R. P. Singh, S. S. Jolly, *J. Sol-Gel Sci. Technol.* **2020**, *94*, 505; b) A. Singh, A. K. Dubey, *ACS Appl. Bio Mater.* **2018**, *1*, 3;

c) H. Kim, S. Mondal, S. Bharathiraja, P. Manivasagan, M. S. Moorthy, J. Oh, *Ceram. Int.* **2018**, *44*, 6062.
[3] J. Sans, M. Arnau, F. Estrany, P. Turon, C. Alemán, *Adv. Mater. Interfaces* **2021**, *8*, 2100163.
[4] J. Sans, J. Llorca, V. Sanz, J. Puiggalí, P. Turon, C. Alemán, *Langmuir* **2019**, *35*, 14782.
[5] a) S. Tarafder, S. Bodhak, A. Bandyopadhyay, S. Bose, *J. Biomed. Mater. Res.* **2011**, *97B*, 306; b) F. Vasquez-Sancho, A. Abdollahi, D. Damjanovic, G. Catalan, *Adv. Mater.* **2018**, *30*, 1705316; c) S. Bose, G. Fielding, S. Tarafder, A. Bandyopadhyay, *Trends Biotechnol.* **2013**, *31*, 594.
[6] a) S. Bodhak, S. Bose, A. Bandyopadhyay, *J. Am. Ceram. Soc.* **2011**, *94*, 1281; b) J. T. B. Ratnayake, M. Mucalo, G. J. Dias, *J. Biomed. Mater. Res., Part B* **2017**, *105*, 1285.
[7] E. Fukada, I. Yasuda, *J. Phys. Soc. Japan* **1957**, *12*, 1158.
[8] a) C. S. Ciobanu, S. L. Iconaru, M. C. Chifiriuc, A. Costescu, P. L.e Coustumer, D. Predoi, *Biomed Res. Int.* **2013**, *2013*, 916218; b) S. Zhao, C. Guo, Y.-Z. Hu, Y.-R. Guo, Q.-J. Pan, *Open Chem.* **2018**, *16*, 20.
[9] C. Prakash, S. Singh, B. S. Pabla, M. S. Uddin, *Surf. Coatings Technol.* **2018**, *346*, 9.
[10] a) X. Zhang, M. Z. Yates, *ACS Appl. Mater. Interfaces* **2018**, *10*, 17232; b) R. Munirathinam, D. Pham Minh, A. Nzihou, *Int. J. Hydrogen Energy* **2020**, *45*, 18440.
[11] M. Rivas, L. J. del Valle, E. Armelin, O. Bertran, P. Turon, J. Puiggalí, C. Alemán, *ChemPhysChem* **2018**, *19*, 1746.
[12] T. Kobayashi, S. Nakamura, K. Yamashita, *J. Biomed. Mater. Res.* **2001**, *57*, 477.
[13] M. Ueshima, S. Tanaka, S. Nakamura, K. Yamashita, *J. Biomed. Mater. Res.* **2002**, *60*, 578.
[14] J. Sans, G. Revilla-López, V. Sanz, J. Puiggalí, P. Turon, C. Alemán, *Chem. Commun.* **2021**, *57*, 5163.
[15] J. Sans, V. Sanz, L. J. del Valle, J. Puiggalí, P. Turon, C. Alemán, *J. Catal.* **2021**, *397*, 98.
[16] a) N. Horiuchi, S. Nakaguki, N. Wada, K. Nozaki, M. Nakamura, A. Nagai, K. Katayama, K. Yamashita, *J. Appl. Phys.* **2014**, *116*, 014902; b) N. Horiuchi, M. Nakamura, A. Nagai, K. Katayama, K. Yamashita, *J. Appl. Phys.* **2012**, *112*, 074901; c) M. Nakamura, N. Hori, S. Namba, T. Toyama, N. Nishimiya, K. Yamashita, *Biomed. Mater.* **2015**, *10*, 011001.
[17] a) M. H. Fathi, A. Hanifi, V. Mortazavi, *J. Mater. Process. Technol.* **2008**, *202*, 536; b) A. Z. Alshemary, Y. Goh, M. Akram, M. R. A. Kadir, R. Hussain, *Sci. Adv. Mater.* **2015**, *7*, 249.
[18] J. Sans, E. Armelin, V. Sanz, J. Puiggalí, P. Turon, C. Alemán, *J. Catal.* **2020**, *389*, 646.
[19] S. Ou, S. Chiou, K. Ou, *Ceram. Int.* **2013**, *39*, 3809.
[20] S. Nakamura, H. Takeda, K. Yamashita, *J. Appl. Phys.* **2001**, *89*, 5386.
[21] F. Müller, C. A. Ferreira, D. S. Azambuja, C. Alemán, E. Armelin, *J. Phys. Chem. B* **2014**, *118*, 1102